Two active-electron classical trajectory Monte Carlo methods for ion-He collisions

F. Guzmán,[1] L. F. Errea,[1] and B. Pons[2]
[1]*Departamento de Química C-IX, Universidad Autónoma de Madrid, 28049 Madrid, Spain*
[2]*CELIA, Université de Bordeaux I–CRNS–CEA, 351 Cours de la Libération, 33405 Talence, France*
(Received 17 July 2009; published 16 October 2009)

We introduce two active-electron classical trajectory Monte Carlo models for ion-He collisions, in which the electron-electron force is smoothed using a Gaussian kernel approximation for the pointwise classical particles. A first model uses independent pairs of Gaussian electrons, while a second one employs time-dependent mean-field theory to define an averaged electron-electron repulsion force. These models are implemented for prototypical p+He collisions and the results are compared to available experimental and theoretical data.

DOI: 10.1103/PhysRevA.80.042708 PACS number(s): 34.10.+x, 34.70.+e, 34.80.Dp, 31.15.xv

I. INTRODUCTION

The classical trajectory Monte Carlo (CTMC) method has been successfully applied during the past decades to the study of dynamical processes in one-electron ion-atom collisions (see, e.g., [1–5] and references therein). This method is particularly useful in the intermediate impact velocity range roughly characterized by $1 \lesssim v/v_e \lesssim 3$, where v and v_e are, respectively, the projectile velocity and the orbital speed of the electron in its initial state, since standard semiclassical approaches, which quantum mechanically describe the electron motion by expanding the total wave function on atomic or molecular basis sets, face difficulties in describing the strong competition among capture, excitation, and ionization mechanisms in this velocity regime [6–8]. Moreover, CTMC calculations provide at about $v/v_e \sim 1$ total and partial cross sections that adequately coalesce with those obtained by means of semiclassical techniques [9]; CTMC and semiclassical results can therefore be merged to yield recommended cross sections over a wide range of impact energies ($E \sim 1-1000$ keV/amu) of interest for fusion plasma diagnostics using neutral beams [9,10].

Extension of CTMC calculations to two-electron targets have mainly been performed within the independent electron model (IEM) [11,12] using an effective charge [5,13,14] or a static model potential [15] to represent the interaction of the active electron with the frozen target core. Some agreement with experimental data has been obtained for single capture and single ionization, while double processes have systematically been overestimated [5,15,16], as expected from semiclassical analysis of multielectronic probabilities and corresponding couplings [17,18].

Attempts have therefore been made to explicitly consider all target electrons in the CTMC description of collisional dynamics. Most of the works considered the prototypical He target, whose classical description generally leads to unphysical autoionization, even in the absence of external perturbation. Kirschbaum and Wilets [19] remedied this by adding to the He Hamiltonian a repulsive potential, motivated by the Heisenberg uncertainty principle which constrains the phase-space coordinates $\{\mathbf{r_i}, \mathbf{p_i}\}$ of the electrons to $r_i p_i \geq \xi$, where ξ is a free parameter of order 1 in atomic units. Alternatively, Cohen introduced the energy-bounded approach [20] in which autonization is precluded by means of a repulsive potential that prevents electrons from getting too bounded while others are ejected. Montemayor and Schiwietz [21] rather drew from the usual IEM and developed a dynamical screening CTMC (dCTMC) approach in which the electron-electron repulsion is represented in terms of a time-dependent model potential in which a bound, yet active, electron screens the target potential viewed by the other active electron. This approach has been extended in [22] to account for screening around the projectile when both electrons are subject to capture.

In the present work, we first propose a statistical CTMC method that does not involve any repulsive potential, but assimilates the two active electrons to Gaussian density distributions for the calculation of the electron-electron repulsion force. This leads to a regularization of the Coulombian interaction that stabilizes the He system and enables the study of ion-He dynamics in terms of independent couples of $\{\mathbf{r_i}, \mathbf{p_i}, i=1,2\}$ electronic trajectories. We shall refer to this method as independent pairs of Gaussian electrons (IPGE). We shall also consider a CTMC method in which all classical trajectories evolve simultaneously and where the repulsive force that each classical electron experiences results from the (regularized) interaction with the entire set of trajectories that represent the other electron. This latter approach shall be labeled averaged collective repulsion (ACR) and its collective character makes it closer to quantum-mechanical mean-field treatments of two-electron dynamics than IPGE.

These two methods will be applied to the description of the following single- and double-electron processes

$$\mathrm{He}(1s^2) + \mathrm{H}^+ \rightarrow \mathrm{He}^+ + \mathrm{H} \quad \text{single capture}, \tag{1a}$$

$$\rightarrow \mathrm{He}^+ + \mathrm{H}^- \quad \text{double capture}, \tag{1b}$$

$$\rightarrow \mathrm{He}^+ + \mathrm{H}^+ + e^- \quad \text{single ionization}, \tag{1c}$$

$$\rightarrow \mathrm{He}^{2+} + \mathrm{H}^+ + 2e^- \quad \text{double ionization}, \tag{1d}$$

$$\rightarrow \mathrm{He}^{2+} + \mathrm{H} + e^- \quad \text{transfer ionization}, \tag{1e}$$

from low ($E=10$ keV) to high ($E=1000$ keV) impact energies.

Our paper is organized as follows. After briefly reviewing the stability conditions for the isolated He atom in Sec. II A, we, respectively, present the IPGE and ACR approaches in Secs. II B and II C. Section III contains our dynamical results, and conclusions are given in Sec. IV. Atomic units are used throughout unless otherwise stated.

II. METHODS

We employ the impact-parameter approximation [23] where the (bare) projectile of nuclear charge Z_P follows a rectilinear trajectory $\mathbf{R}(t)$ with constant velocity $\mathbf{v}$ and impact parameter $\mathbf{b}$ so that $\mathbf{R}(t)=\mathbf{b}+\mathbf{v}t$. The total Hamiltonian H is split as $H=H_T+V_P$, where

$$H_T = H_0 + V_R \equiv \left[\sum_{i=1}^{2} \frac{\mathbf{p}_i^2}{2} - \frac{Z_T}{r_i}\right] + \frac{1}{|\mathbf{r}_1 - \mathbf{r}_2|} \tag{2}$$

is the unperturbed target Hamiltonian, $\mathbf{r}_i$ and $\mathbf{p}_i$ $(i=1,2)$ are the spatial and momentum coordinates of the two electrons, $Z_T=2$, and

$$V_P = -\sum_{i=1}^{2} \frac{Z_P}{|\mathbf{r}_i - \mathbf{R}|} \tag{3}$$

corresponds to the electron-projectile interactions. The two-electron phase-space distribution $\varrho(\mathbf{r}_1,\mathbf{p}_1,\mathbf{r}_2,\mathbf{p}_2,t)$ consists of the product

$$\varrho(\mathbf{r}_1,\mathbf{p}_1,\mathbf{r}_2,\mathbf{p}_2,t) = \varrho_1(\mathbf{r}_1,\mathbf{p}_1,t)\varrho_2(\mathbf{r}_2,\mathbf{p}_2,t) \tag{4}$$

and each $\varrho_i(\mathbf{r}_i,\mathbf{p}_i,t)$ (with $i=1,2$) is discretized in terms of N trajectories, yielding N^2 two-electron configurations whose dynamics are classically described by the Hamilton equations [24]

$$\dot{\mathbf{r}}_i \cdot \mathbf{e}_\alpha = \frac{\partial H}{\partial \mathbf{p}_i \cdot \mathbf{e}_\alpha}, \tag{5}$$

$$\dot{\mathbf{p}}_i \cdot \mathbf{e}_\alpha = -\frac{\partial H}{\partial \mathbf{r}_i \cdot \mathbf{e}_\alpha}, \tag{6}$$

where $\mathbf{e}_\alpha$ stands for one of the usual Cartesian unitary vectors $(\alpha=x,y,z)$.

A. Isolated helium atom

When $Z_P=0$, the only classical trajectories that remain unconditionally stable are those whose initial positions are symmetric with respect to the target nucleus (where the origin of electronic coordinates is located)

$$\mathbf{r}_1 = -\mathbf{r}_2, \tag{7}$$

$$\mathbf{p}_1 = -\mathbf{p}_2, \tag{8}$$

so that all forces, including the electron-electron repulsive one, are central. To define the initial condition for each pair of electrons, we locate one electron at the aphelion of an ellipsis that would correspond, in the one-electron case, to the distance from the nucleus [1]

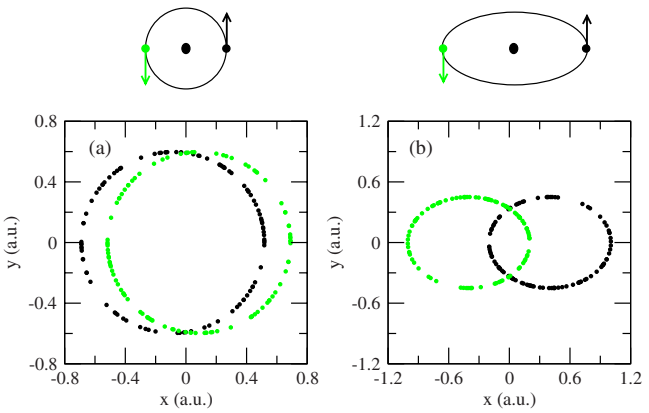

FIG. 1. (Color online) Temporal evolution of stable configurations of classical He atom. The electronic trajectories are initially defined (a) circular and (b) elliptic, with $\beta=1$ and 0.5, respectively [see Eqs. (11) and (12)], as schematized in the upper figures (which are not scaled with the lower ones). Green (light gray) and black (dark) symbols, respectively, refer to electrons 1 and 2. The selected configurations pertain to the (x,y) plane with the He nucleus located at (0,0).

$$r_1 = \frac{-Z_T(1+\sqrt{1-\beta})}{2E_m}, \tag{9}$$

where E_m is the energy associated with the one-electron part of the Hamiltonian H_T and $\beta=l^2/l_{max}^2$ is the angular-momentum parameter with $0\le\beta\le1$. E_m depends on r_1 and is related to the total energy E_T of the He atom in the symmetric configuration by

$$E_T = 2E_m + \frac{1}{2r_1}. \tag{10}$$

Substitution of E_m in Eq. (9) leads to

$$r_1 = \frac{-2Z_T(1+\sqrt{1-\beta})+1}{2E_T} = r_2, \tag{11}$$

with associated velocities of magnitude

$$v_1 = \sqrt{E_T - \frac{1}{2r_1}(1-4Z_T)} = v_2. \tag{12}$$

N initial conditions for electron 1 are thus randomly distributed in phase space according to Eqs. (11) and (12), with $\mathbf{r}_1 \perp \mathbf{v}_1$ and $\beta \in [0,1]$. The symmetry constraints (8) reduce the dimension of the two-electron distribution (4) to N. In Fig. 1, we illustrate the stability of symmetric He for the cases of trajectories initially defined circular $(\beta=1)$ and elliptic $(\beta=0.5)$. The initial (one-electron) character of the trajectories is modified by the repulsive force but the two-electron system remains stable since the symmetry conserves the central (radial) nature of all electrostatic forces.

Although all pairs of symmetric trajectories in the isolated He atom are stationary, the presence of any small perturbation makes this system classically unstable. We have verified this by placing a proton $Z_P=1$ at 100 a.u. from the He center. The scenario for unphysical autoionization is displayed in Fig. 2, considering initial circular trajectories as an example:

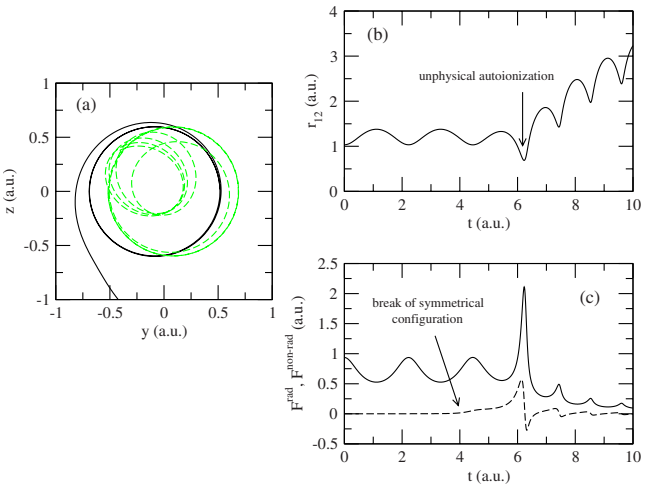

FIG. 2. (Color online) (a) Temporal evolution in the (y,z) plane of the initially stable circular electron configuration of classical He atom, perturbed by a proton fixed at $(y=0,\ z=100)$; the continuous black and dashed green lines correspond to the two electron planar trajectories. (b) Interelectronic distance r_{12} as function of time t. (c) Radial (—) and nonradial (- - -) parts of the interelectronic force.

the electrostatic perturbation breaks the symmetry of the motions of the electrons so that the repulsive electron-electron force rapidly exhibits a nonradial component [for $t>4$ a.u. in Fig. 2(c)]; the electronic trajectories are then severely perturbed [see Fig. 2(a)] and both radial and nonradial components of the force present sharp peaks as the electrons come close to each other [see Figs. 2(b) and 2(c)]. This leads to a drastic increase of their kinetic energy which cannot be counterbalanced by the nuclear potential. Unphysical autoionization thus follows at about $t=6.2$ a.u. in Fig. 2.

B. IPGE

A way to preserve stability in the classical He atom is to soften the short-range behavior of the electron-electron repulsive force. We have implemented the Gaussian kernel approximation (GKA) in which the classical electrons are described in terms of Gaussian functions, of width σ_r, centered on the positions of the corresponding pointwise particles. The electron i, located at $\mathbf{r}_i$ at time t, is then represented by the charge distribution

$$f_i(\mathbf{r},t)=\frac{1}{(2\pi)^{3/2}\sigma_r^3}\exp\left\{-\frac{[\mathbf{r}-\mathbf{r}_i(t)]^2}{2\sigma_r^2}\right\}, \tag{13}$$

which is normalized so that $\int d\mathbf{r} f_i(\mathbf{r},t)=1$ and travels with momentum $\mathbf{p}_i$ conjugate to $\mathbf{r}_i$. This approximation is quite usual in molecular-dynamics studies of complex systems (see, e.g., [25–27]). In a first step, we only used the GKA to compute the repulsive potential and corresponding force, acting between the electrons. Furthermore, the potential felt by electron 1, and due to electron 2, is calculated by assuming that electron 1 is pointwise while electron 2 is Gaussian. This yields

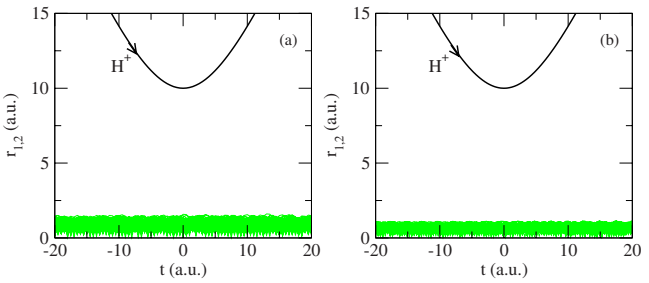

FIG. 3. (Color online) Electron-target distances $r_{1,2}(t)$, as functions of time t, for some randomly sorted trajectories in microcanonical (a) IPGE and (b) ACR calculations of p+He collisions with $v=1$ a.u. and $b=10$ a.u.. The thick black line corresponds to the projectile trajectory $R(t)=|b+vt|$.

$$V_{12}^{\mathrm{IPGE}}(\mathbf{r}_1,\mathbf{r}_2;t)=\int d\mathbf{r} f_2(\mathbf{r},t)\frac{1}{|\mathbf{r}-\mathbf{r}_1|}=\frac{1}{r_{12}}\mathrm{erf}\left(\frac{r_{12}}{\sqrt{2}\sigma_r}\right) \tag{14}$$

and the corresponding force, entering the Hamilton's Eq. (6),

$$\mathbf{F}_{12}^{\mathrm{IPGE}}(\mathbf{r}_1,\mathbf{r}_2;t)=(\nabla_{\mathbf{r}_1}r_{12})\left[\frac{1}{r_{12}^2}\mathrm{erf}\left(\frac{r_{12}}{\sqrt{2}\sigma_r}\right)-\sqrt{\frac{2}{\pi}}\frac{1}{\sigma_r r_{12}}e^{-r_{12}^2/2\sigma_r^2}\right], \tag{15}$$

where $\mathbf{r}_1\equiv\mathbf{r}_1(t)$ and $\mathbf{r}_2\equiv\mathbf{r}_2(t)$ are the coordinates of the electrons, $\mathbf{r}_{12}=\mathbf{r}_1-\mathbf{r}_2$, and $\mathrm{erf}(x)=\frac{2}{\sqrt{\pi}}\int_0^x e^{-u^2}du$. While $\mathbf{F}_{12}^{\mathrm{IPGE}}\to\hat{\mathbf{r}}_{12}/r_{12}^2$ as $r_{12}\gg\sigma_r$, GKA softening operates in Eq. (15) through $\mathbf{F}_{12}^{\mathrm{IPGE}}\to\mathbf{0}$ as $r_{12}\to 0$ since $\mathrm{erf}(x)\to\frac{2}{\sqrt{\pi}}x$ for $x\to 0$. As a consequence of this softening, stable two-electron He configurations can be obtained beyond the symmetry restriction of the previous unscreened case. The value of the parameter σ_r is selected under the requirement that all random N^2 pairs of two-electron trajectories, including nonsymmetric ones, remain stable. In practice, we found that $\sigma_r\geq 1$ is adequate and all the following IPGE dynamical results correspond to $\sigma_r=1$. We demonstrate in Fig. 3(a) that GKA indeed affords stability to classical He, in the case of p+He collision with $v=1$ a.u. and $b=10$ a.u., where capture and ionization can be ignored and both electrons are accordingly expected to remain bound to the target. We effectively obtain that $r_{1,2}\leq 2$ a.u. throughout the collision in Fig. 3(a).

In a second step, we also employed GKA for the computation of electron-target (V_T) and electron-projectile (V_P) interactions and considered both electrons to be of Gaussian type in the computation of the electron-electron repulsion. Such calculations lead to dynamical results almost identical to those obtained by means of the IPGE method where GKA is only employed in the computation (15) of $\mathbf{F}_{12}$. Further, they do not permit decreasing the value of σ_r previously selected. The results presented in the next section accordingly refer to the former IPGE method.

Concerning the initial conditions, we define $\varrho_{1,2}(\mathbf{r},\mathbf{p},t\to-\infty)$ as microcanonical sets, of dimension N, corresponding to the $1s$ state of a one-electron system with nuclear charge $Z_T=2$ and energy E'. E' is fixed so that the mean first

ionization potential $\langle I_P\rangle_{\varrho_i}=-\langle p^2/2-Z_T/r+V_{12}^{\mathrm{IPGE}}\rangle_{\varrho_i}$, calculated among the N trajectories belonging to ϱ_i, equals the experimental one, −0.903 a.u.. For $\sigma_r=1$, $E'=-1.39$. Integration of the unperturbed Hamilton's equations (6), with $Z_P=0$ and $\mathbf{F}_{12}^{\mathrm{IPGE}}$ given in Eq. (15), maintains $\langle I_P\rangle_{\varrho_i}$ constant.

When $Z_P\neq 0$, electron trajectories are propagated, for given v and b, up to t_{max}, large enough so that all inelastic processes have terminated. For each IPGE, we then calculate the energies of the electrons with respect to the target, $E_i^T=p_i^2/2-Z_T/r_i$, and to the projectile, $E_i^P=(\mathbf{p}_i-\mathbf{v})^2/2-Z_P/|\mathbf{r}_i-\mathbf{R}|$, with $i=1$ or 2, to discriminate between excited (including elastic), captured, and freed trajectories by means of the respective energy criteria $(E_i^T<0,\ E_i^P>0)$, $(E_i^T>0,\ E_i^P<0)$, and $(E_i^T>0,\ E_i^P>0)$. The inelastic probabilities for all the processes listed in Eq. (1) are finally calculated as

(i) Single capture (SC):

$$P^{(\mathrm{SC})}=\frac{1}{N^2}\sum_{j_1,k_2=1}^{N}\delta_{j_1,c}^{(j_1,k_2)}\delta_{k_2,e}^{(j_1,k_2)}+\delta_{j_1,e}^{(j_1,k_2)}\delta_{k_2,c}^{(j_1,k_2)}.$$

(ii) Double capture (DC):

$$P^{(\mathrm{DC})}=\frac{1}{N^2}\sum_{j_1,k_2=1}^{N}\delta_{j_1,c}^{(j_1,k_2)}\delta_{k_2,c}^{(j_1,k_2)}.$$

(iii) Single ionization (SI):

$$P^{(\mathrm{SI})}=\frac{1}{N^2}\sum_{j_1,k_2=1}^{N}\delta_{j_1,i}^{(j_1,k_2)}\delta_{k_2,e}^{(j_1,k_2)}+\delta_{j_1,e}^{(j_1,k_2)}\delta_{k_2,i}^{(j_1,k_2)}.$$

(iv) Double ionization (DI):

$$P^{(\mathrm{DI})}=\frac{1}{N^2}\sum_{j_1,k_2=1}^{N}\delta_{j_1,i}^{(j_1,k_2)}\delta_{k_2,i}^{(j_1,k_2)}.$$

(v) Transfer ionization (TI):

$$P^{(\mathrm{TI})}=\frac{1}{N^2}\sum_{j_1,k_2=1}^{N}\delta_{j_1,c}^{(j_1,k_2)}\delta_{k_2,i}^{(j_1,k_2)}+\delta_{j_1,i}^{(j_1,k_2)}\delta_{k_2,c}^{(j_1,k_2)}.$$

(vi) Excitation (including elastic) (E):

$$P^{(E)}=\frac{1}{N^2}\sum_{j_1,k_2=1}^{N}\delta_{j_1,e}^{(j_1,k_2)}\delta_{k_2,e}^{(j_1,k_2)}.$$

where, $\delta_{i_j,\alpha}^{(i_j,l_k)}=1$(otherwise 0) indicates that electron i of set j has been ascribed to excitation ($\alpha=e$), capture ($\alpha=c$), or ionization ($\alpha=i$) at the end of the dynamics of the (i_j,l_k) IPGE. For DC, we further verified that the total (two-electron) energy with respect to the projectile, $E_1^P+E_2^P+V_{12}^{\mathrm{IPGE}}$, is negative; similarly, we checked that $E_1^T+E_2^T+V_{12}^{\mathrm{IPGE}}<0$ for the excitation channel. In the framework of the impact-parameter model, the cross sections are obtained according to $\sigma^{(X)}(v)=2\pi\int dbbP^{(X)}(b,v)$.

C. ACR

Alternatively to the IPGE method, we developed a time-dependent mean-field CTMC method for two-electron systems, in which the repulsion force that an electron experiences stems from its interaction with the entire density of the other electron. The resulting repulsive potential is therefore local, as in the quantum model-potential or density-functional approaches [28]. Considering the electron 1 subject to the repulsion of the whole electronic distribution $\varrho_2(\mathbf{r},\mathbf{p},t)$,

$$V_{12}(\mathbf{r}_1;t)=\int d\mathbf{r}\rho_2(\mathbf{r},t)\frac{1}{|\mathbf{r}_1-\mathbf{r}|},\tag{16}$$

where $\rho_2(\mathbf{r},t)=\int d\mathbf{p}\varrho_2(\mathbf{r},\mathbf{p},t)$ [see Eq. (4)]. If we assume that for $t\to-\infty$, the two electrons are equivalent and can be described by $1s$-like (isotropic) microcanonical space densities $\rho_1(r,t\to-\infty)\equiv\rho_2(r,t\to-\infty)$, it is clear from Eq. (16) that $V_{12}(\mathbf{r},t\to-\infty)$ is radial. Concretely, we start from one-electron phase-space distributions $\varrho_{1,2}(\mathbf{r},\mathbf{p},t\to-\infty)=\delta[E_0-p^2/2+Z_T/r-V_{12}(r,t\to-\infty)]$ and derive the spatial densities $\rho_{1,2}(r,t\to-\infty)=(4\pi)^2r^2\int dpp^2\varrho_{1,2}(\mathbf{r},\mathbf{p},t\to-\infty)$, using well-known properties of the δ distribution, as

$$\rho_{1,2}(r,t\to-\infty)=\mathcal{N}r^2\sqrt{\frac{Z_T}{r}-V_{12}(r;t\to-\infty)+E_0},\tag{17}$$

where $\mathcal{N}$ is a normalization factor and $E_0=-0.903$. The interaction potential $V_{12}(r;t\to-\infty)$ defined in Eq. (16) then results

$$V_{12}(r;t\to-\infty)=\frac{1}{r}\int_0^r\rho_{1,2}(r',t\to-\infty)dr'+\int_r^\infty\frac{\rho_{1,2}(r',t\to-\infty)}{r'}dr'.\tag{18}$$

Equations (17) and (18) are self-consistently resolved, by means of an iterative procedure that employs the classical $\mathrm{He}^+(1s)$ spatial density, $\rho_i(r,t\to-\infty)=\mathcal{N}r^2\sqrt{\frac{2}{r}-2}$, as initial guess, to obtain self-consistent-field (SCF) initial conditions. Converged $\rho_{1,2}(r,t\to-\infty)$ and $V_{12}(r;t\to-\infty)$ are drawn in Fig. 4(a) as functions of the radial coordinate r. $\varrho_{1,2}(\mathbf{r},\mathbf{p},t\to-\infty)$ are then discretized in terms of N trajectories using the method of [15] designed for non-Coulombic potentials. This discretization transforms Eq. (16) into

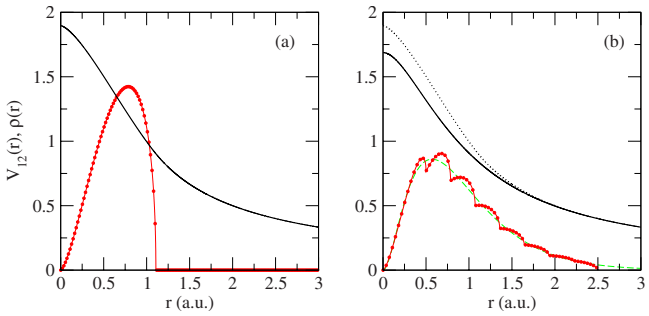

FIG. 4. (Color online) Radial electron densities (red ●—●) and screening potentials (black —) corresponding to the initial conditions in (a) microcanonical ACR calculations [see Eqs. (17) and (18)] and (b) improved ACR model [see Eq. (24)]. In (b), the dashed green line corresponds to the RHF $r^2|\phi(r)|^2$ quantum radial density and the dotted black line represents the microcanonical SCF-ACR screening potential that can be compared to $V^{(\mathrm{RHF})}$.

$$V_{12}(\mathbf{r}_1;t) = \frac{1}{N}\sum_{k_2=1}^{N} \frac{1}{|\mathbf{r}_1 - \mathbf{r}_{k_2}|}, \tag{19}$$

where $\mathbf{r}_{k_2}$, with $k_2=1,\ldots,N$, corresponds to the positions at time t of the N trajectories belonging to the discretized set ϱ_2. These N pointwise contributions, randomly distributed in phase space, cannot reproduce the perfect initial isotropy of ϱ_2 (except as $N\to\infty$). As a result, neither V_{12}, computed according to Eq. (19), nor $\mathbf{F}_{12}$, with $\mathbf{F}_{12}=-\boldsymbol{\nabla}V_{12}$, are perfectly radial so that artificial autoionization can occur as soon as the Hamilton's equations are propagated.

To overcome this computational inconvenience, we calculate within each microcanonical set ϱ_i the time-dependent energy of electron j, $E_j(t)=p_j^2/2-Z_T/r_j+V_{12}(r_j,t\to-\infty)$, and state that electron j still pertains to the elastic channel, and thus contributes to the e-e repulsion according to $V_{12}(r,t\to-\infty)$, if $E_j(t)\leq E_0+\Delta E$, where $E_0=-0.903$ and ΔE is small ($\sim$0.05) and allows for insignificant numerical deviations upon integration of the Hamilton's equations. Let $N_{\text{entry}}^{(i)}(t)$ be the number of electrons which belong to the entry channel at time t within the set i. The mutual e-e interaction potential acting on electron 1, and due to the whole set ϱ_2, is then defined as

$$V_{12}^{\text{ACR-}m}(\mathbf{r}_1;t) = \frac{1}{N}\Bigg[N_{\text{entry}}^{(2)}(t) V_{12}(r_1;t\to-\infty) + \sum_{j_2, E_{j_2}>E_0+\Delta E} V_{12}^{\text{IPGE}}(\mathbf{r}_1,\mathbf{r}_2;t)\Bigg], \tag{20}$$

where the GKA has been employed to smooth the nonelastic part of the one-electron distribution $\varrho_2(\mathbf{r},t)$, yielding the V_{12}^{IPGE} contributions (14) to the total $V_{12}^{\text{ACR-}m}$. The value of the smoothing parameter σ_r entering V_{12}^{IPGE} in Eq. (20) is chosen as small as possible; in practice, we have examined the $0.2\leq\sigma_r\leq1$ range and shall demonstrate the noticeable stability of the cross sections within this range. It is worth noting that the lower bound value $\sigma_r=0.2$ is significantly lower than the one used in IPGE. We show in Fig. 3(b) that the present mean-field ACR approach with $\sigma_r=0.2$ brings stability to He, in case of distant p+He collisions with $v=1$ a.u. and $b=10$ a.u., where no significant inelastic processes are expected to occur.

The self-consistent initial conditions (17) and (18) lead to a short-range spatial density limited to $r\leq1.17$ as shown in Fig. 4(a). Such contraction, inherent in any microcanonical description, is known to yield underestimated cross sections in the low and intermediate impact velocity ranges of one-electron ion-atom collisions [3,5]. Improved descriptions rely on a better representation of the quantum density and particularly of the tail of the spatial electronic distribution from which electrons are preferentially pulled out (see, e.g., [3,29]). In this work, the quantum reference consists of the Roothan-Hartree-Fock (RHF) description of He [30] in terms of a product of one-electron single-χ wave functions

$$\phi_{1,2}^{(\text{RHF})}(\mathbf{r}) = \frac{\chi^{3/2}}{\pi^{1/2}}\exp(-\chi r), \tag{21}$$

with $\chi=1.6875$. To classically describe $|\phi_{1,2}^{(\text{RHF})}(\mathbf{r})|^2$ within the $0\leq r\leq2.5$ range beyond which $|\phi_{1,2}^{(\text{RHF})}(\mathbf{r})|^2\sim0$ [see Fig. 4(b)], we follow guidelines of previous works (see, e.g., [3,29]) and build a linear combination of M He^+-like microcanonical sets of different energies E_k,

$$\varrho_{1,2}^{(\text{RHF})}(\mathbf{r},\mathbf{p}) = \sum_{k=1}^{M=8} a_k \varrho_k^{(\text{He}^+)}(\mathbf{r},\mathbf{p}), \tag{22}$$

so that $\rho_{1,2}^{(\text{RHF})}(\mathbf{r})=\int d\mathbf{p}\,\varrho_{1,2}^{(\text{RHF})}(\mathbf{r},\mathbf{p})$ least-squares fits $|\phi_{1,2}^{(\text{RHF})}(\mathbf{r})|^2$. In Eq. (22), M has been arbitrarily chosen equal to 8 and the energies E_k are fixed so that the corresponding maximal radii $r_{max,k}$ of the one-electron $\varrho_k^{(\text{He}^+)}$, which fulfill $r_{max,k}=2/|E_k|$, verify $r_{max,k}=2.5k/M$. We illustrate in Fig. 4(b) how $\rho_{1,2}^{(\text{RHF})}(r)$ succeeds in describing the tail of $|\phi_{1,2}^{(\text{RHF})}(r)|^2$ up to $r=2.5$ a.u.. The mutual e-e screening potential is then obtained as in Eq. (18), with $\rho_{1,2}(r',t\to-\infty)$ changed into $4\pi r^2|\phi_{1,2}^{(\text{RHF})}(r')|^2$, or equivalently into $\rho_{1,2}^{(\text{RHF})}(r')$ since $\rho_{1,2}^{(\text{RHF})}(r')\sim4\pi r^2|\phi_{1,2}^{(\text{RHF})}(r')|^2$, to yield

$$V^{(\text{RHF})}(r) = \frac{1-(1+\chi r)\exp(-2\chi r)}{r} \tag{23}$$

as in [21]. $V^{(\text{RHF})}(r)$ slightly differs from the previous SCF interaction potential in the inner $r\leq1.5$ a.u. range [see Fig. 4(b)]. Improved initial conditions, with one-electron spatial densities drawing near to $\phi_{1,2}^{(\text{RHF})}(\mathbf{r})$ and accounting for mutual screening through (23), are finally obtained as linear combinations of microcanonical distributions corresponding to the non-Coulombic potential $-Z_T/r+V^{(\text{RHF})}(r)$,

$$\varrho_{1,2}^{(c)}(\mathbf{r},\mathbf{p};t\to-\infty) = \sum_{k=1}^{M=8} a_k \varrho_k^{(-Z_T/r+V^{(\text{RHF})})}(\mathbf{r},\mathbf{p}), \tag{24}$$

where each $\varrho_k^{(-Z_T/r+V^{(\text{RHF})})}$ are constructed following the procedure described in [15]. $\varrho_{1,2}^{(c)}$ only slightly differ from $\varrho_{1,2}^{(\text{RHF})}$ so that the present procedure can also be interpreted as SCF, yet iterations are stopped at the first step. With respect to the subsequent time propagation, we follow a procedure similar to Eq. (20) with the mutual e-e interaction potential

$$V_{12}^{\text{ACR-}c}(\mathbf{r}_1;t) = \frac{1}{N}\Bigg[N_{\text{entry}}^{(2)}(t) V^{(\text{RHF})}(r_1) + \sum_{j_2, E_{j_2}>E_M+\Delta E} V_{12}^{\text{IPGE}}(\mathbf{r}_1,\mathbf{r}_2;t)\Bigg], \tag{25}$$

where $N_{\text{entry}}^{(2)}(t)$ corresponds to the number of electrons of set 2 belonging to the entry channel at time t, i.e., electrons fulfilling $E_j(t)=p_j^2/2-Z_T/r_j+V^{(\text{RHF})}(r_j)\leq E_M+\Delta E$, with $E_M\sim-0.4$, the energy of the most excited microcanonical distribution forming the improved initial conditions (24).

From a computational point of view, the present ACR approach entangles the dynamics of the two electrons through Eq. (19) so that the number of Hamilton's equations to be solved reduces to $12N$. Nonetheless, all these $12N$ equations have to be solved simultaneously as a function of

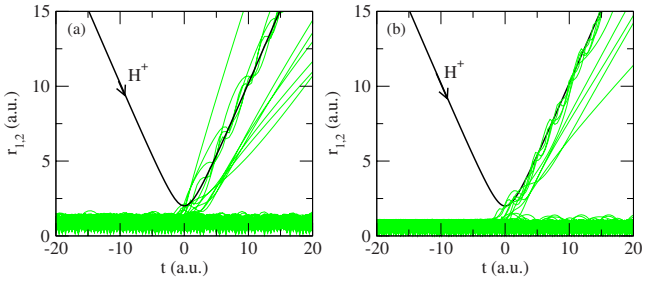

FIG. 5. (Color online) Electron-target distances $r_{1,2}(t)$, as functions of time t, for some randomly sorted trajectories in microcanonical (a) IPGE and (b) ACR calculations of p+He collisions with $v=1$ a.u. and $b=2$ a.u.. The thick black line corresponds to the projectile trajectory $R(t)=|b+vt|$.

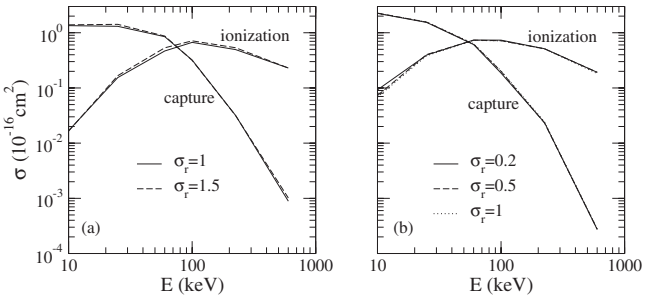

FIG. 6. Single-capture and single-ionization cross sections, as functions of the impact energy E in p+He collisions, computed in the framework of (a) IPGE and (b) ACR methods using various values of σ_r.

time, whereas IPGE consists in solving N^2 independent pairs of 12 coupled Hamilton's equations. To derive the inelastic probabilities at the final integration time t_{max}, we first proceed as in the IPGE framework and calculate, within each ϱ_i set, the energies of the trajectory j with respect to the target, $E_j^T=p_j^2/2-Z_T/r_i$, and to the projectile, $E_j^P=(\mathbf{p}_j-\mathbf{v})^2/2-Z_P/|\mathbf{r}_j-\mathbf{R}|$. When both E_j^T and $E_j^P>0$, trajectory j is ascribed to ionization; capture corresponds to $E_j^T>0$ and $E_j^P<0$ while for excitation (including elastic) processes, $E_j^T<0$ and $E_j^P>0$. Since we do not deal anymore with independent pairs of electrons, we can now easily define single-electron capture P_i^c, excitation P_i^e, and ionization P_i^i probabilities by counting, among the N electrons pertaining to set i, those which fulfill the respective energy criteria. The two-electron probabilities for all the processes listed in Eq. (1) are thus computed according to

(i) SC:

$$P^{(\mathrm{SC})}=P_1^cP_2^e+P_1^eP_2^c.$$

(ii) DC:

$$P^{(\mathrm{DC})}=P_1^cP_2^c.$$

(iii) SI:

$$P^{(\mathrm{SI})}=P_1^iP_2^e+P_1^eP_2^i.$$

(iv) DI:

$$P^{(\mathrm{DI})}=P_1^iP_2^i.$$

(v) TI:

$$P^{(\mathrm{TI})}=P_1^cP_2^i+P_1^iP_2^c.$$

(vi) E:

$$P^{(E)}=P_1^eP_2^e.$$

The corresponding cross sections are still obtained as $\sigma^{(X)}(v)=2\pi\int dbbP^{(X)}(b)$.

III. RESULTS

We present in Fig. 5 the electron-target distances $r_{i_j}(t)$, as functions of time t, for some randomly sorted trajectories in IPGE and microcanonical ACR calculations of p+He collisions with $v=1$ a.u. and $b=2$ a.u.. Ionizing and capture trajectories can be clearly identified: the latter ones coil round the projectile path in the outgoing phase of the collision ($Z=vt>0$), while the former ones missed to be caught by the proton in the inner $Z\sim 0$ region and are mainly emitted in the forward direction because of projectile focusing effect [31]. With respect to Fig. 3, Fig. 5 reinforces the stability afforded by the IPGE and ACR methods: all inelastic processes originate from the so-called molecular region ($Z\sim 0$) and fictitious ionization (or anomalous target excitation) do not arise in either the ingoing ($Z\lesssim -5$ a.u.) or outgoing ($Z\gtrsim 5$ a.u.) parts of the collision.

Before turning our attention to the comparison of our computed cross sections with the existing experimental and theoretical data, it is worthwhile to check how the IPGE and ACR methods provide cross sections stable with respect to the key parameter σ_r. We accordingly present in Figs. 6(a) and 6(b) the single ionization and capture cross sections calculated in the respective IPGE and improved ACR frameworks using increasing values of σ_r. Both methods are clearly not ill conditioned since the results are almost insensitive to σ_r, beyond the specific values ensuring stability of unperturbed He. Similar behavior has been found for the cross sections associated with two-electron processes.

A. Single capture and single ionization

The IPGE and improved ACR cross sections for single capture and ionization in p+He collisions are displayed in Figs. 7(a) and 7(b), as functions of the impact energy E with $10\leq E\leq 1000$ keV. They are compared to the experimental data of Shah *et al.* [32,33] obtained by means of a crossed-beam technique combined with electron-ion and ion-ion coincidence measurements. Figures 7(a) and 7(b) also include the theoretical results of Reinhold and Falcon [15], who employed a static model potential (and related IPM) to describe p+He as an effective one-electron system in the framework of the CTMC method. We also report in Figs. 7(a) and 7(b) the results of Zajfman and Maor [34] and Cohen [20], who independently used the two-electron classical procedure of Kirchbaum and Wilets (KW), as well as the cross sections obtained by means of the two active-electron energy-bounded approach [20]. Wetmore and Olson [35] introduced

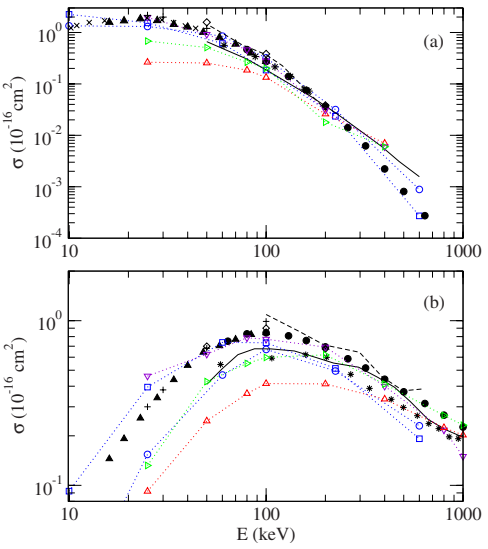

FIG. 7. (Color online) (a) Single-capture and (b) single-ionization cross sections in p+He collisions, as functions of the impact energy E. Present IPGE (○…○) and ACR (□…□) calculations. Previous theoretical results: static model potential CTMC (∗ [15]), ξ=1.257 KW (- - - [34]), ξ=1 KW (△…△ [20]), ξ =1.0844 KW (▷…▷ [20]), two-electron CTMC (— [35]), energy-bounded CTMC (▽…▽ [20]), and semiclassical atomic (+ [36,37]) and (◇ [38]) and molecular (× [39]) calculations. Experiments: ▲ and ● [32,33].

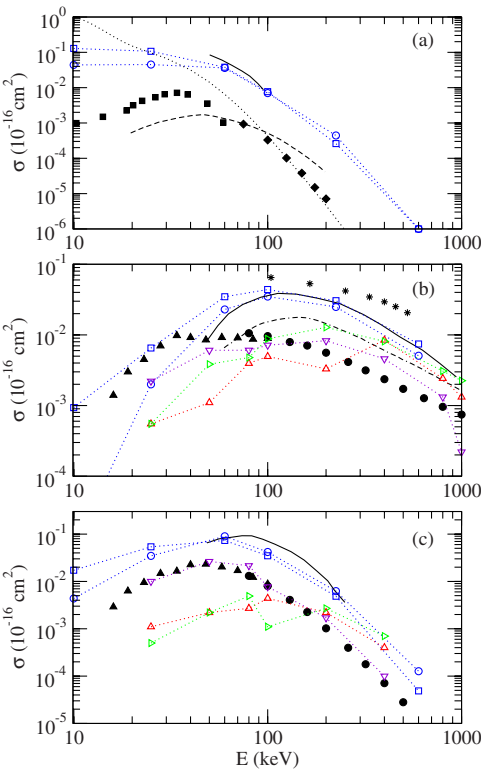

FIG. 8. (Color online) Cross sections for (a) double capture, (b) double ionization, and (c) transfer-ionization processes in p+He collisions as functions of the impact energy E. Present IPGE (○…○) and ACR (□…□) calculations. Previous theoretical results: static (∗ [15]) and time-dependent (- — — - [21]) model potential CTMC, ξ=1 KW (△…△ [20]), ξ=1.0844 KW (▷…▷ [20]), two-electron CTMC (— [35]), energy-bounded CTMC (▽…▽ [20]), semiclassical monopole approximation (- - - [44]), and perturbative CDW (…, [43]) calculations. Experiments: ▲ and ● [32,33], ■ [41], and ◆ [42].

a two-electron CTMC method that does not account for the e-e repulsive force; their results are included in the figures. Semiclassical coupled-state methods have also been applied to the description of p+He collisions; Slim *et al.* [36,37] and Winter [38] employed atomic approaches which consist in expanding the total two-electron wave function on traveling atomic states whereas Errea *et al.* [39] used an expansion in terms of *ab initio* molecular wave functions, especially suited to the description of charge-exchange at low impact energies.

Concerning single capture, most of the theoretical calculations, including the present ones, are in reasonable agreement with the experimental data, even if the classical calculations do not represent the maximum of the cross section around E=25 keV. In this respect, it is to be noted that CTMC-like calculations cannot describe underbarrier transitions which determine a large part of the capture process at low impact energies [23,29]. The KW results significantly depend on the ξ parameter that constrains the electrons to $r_i p_i \geq \xi$: Zajfman and Maor took ξ=1.257 to reproduce the mean electronic momentum obtained from Hartree-Fock calculations, while Cohen successively considered ξ=1 and ξ =1.0844 which, respectively, allow one to obtain correct ionization potentials for He^+ and He.

The agreement between experimental and theoretical results is not as good for single ionization as for capture. The IPGE method yields a cross section in agreement with the static model potential CTMC calculations of Reinhold and Falcon [15] for $E \geq 50$ keV. These results are also close to the two active-electron CTMC results of Wetmore and Olson [35] and to the ξ=1.0844 KW calculations of Cohen. All these computed cross sections are significantly below the measurements of Shah *et al.* [32,33]. In this respect, the improved initial conditions (24) used in the ACR approach lead to a single-ionization cross section in better agreement with the experiments from low to intermediate impact energies. At higher energies, discrepancy with [32,33] still persists; this may be due to the fact that the linear combination (24) of microcanonical distributions does not succeed in representing perfectly the quantum momentum distribution $\phi^{\mathrm{RHF}}(p)$ which determine the ionization process at high E [40].

B. Double capture, double ionization, and transfer ionization

The IPGE and ACR cross sections for H^- formation are presented in Fig. 8(a) and compared to the experimental results of Williams [41] and Toburen and Nakai [42] who both employed the technique based on the dependence on target pressure of I^-/I^+, where I^- and I^+, respectively, stand for H^- and H^+ signal intensities, to determine the double capture cross section. Figure 8(a) also includes the perturbative four-body continuum-distorted-wave (CDW) results of Belkić and Mančev [43], as well as the cross section computed by Lin [44] who used an independent electron approximation to

simplify the computation of the electron-electron interaction in the framework of a three-state two-center atomic expansion. The IPGE and ACR cross sections are quite similar in the whole impact energy range and adequately reproduce the shape of the experimental results, even though our classical calculations lead to a flat shape at low E as for single capture. Nevertheless, our results lie above the experimental data, similar to the two active-electron calculations of Wetmore and Olson [35]. As analyzed in [17,18], such an overestimation could stem from an underestimation of e-e repulsion on the projectile center. In our mean-field ACR approach, the repulsion is indeed averaged over all the N trajectories wherever are centered the corresponding electrons. If such a procedure is well founded in the molecular $Z\sim 0$ region, it soon becomes questionable as the two nuclei recede from each other. For instance, if N_c electrons of one set have been captured by the projectile, one electron of the other set approaching this center feels a repulsion diminished by a factor $\sim N_c/N$ because of Eq. (19). A mean-field procedure that accounts for the location of the electron and the number of electrons trapped by the nuclear centers can be constructed; it would be much more involved than the present one which yields results as accurate as [35]. In the IPGE method, the underestimation of the e-e repulsion comes from the smoothed short-range character of V_{12} [see Eq. (14)]. Smaller values of σ_r would probably remedy this, but they do not stabilize He.

The cross sections for double ionization are presented in Fig. 8(b). The IPGE and ACR approaches yield similar results but the improved initial conditions used in the ACR make the agreement with the experimental data of Shah *et al.* [32,33] better for $E\leq 30$ keV. For higher E, our results, which again coincide with the two-electron CTMC calculations of Wetmore and Olson [35], lie above the measurements. The overestimation is relatively smaller than for double capture and less than the one obtained by means of the static model potential CTMC method [15]. The probable underestimation of e-e repulsion around the projectile center, previously discussed, can be responsible for the observed effect since it underlies an exaggerated pulling force from the projectile when this latter crosses the target. Neither the time-dependent target-screening approach [21] nor the CTMC methods including constraining potentials [20] succeed in fitting the measurements; the latter ones further exhibit structured shapes with respect to E besides the strong dependence on ξ of the KW cross sections.

Finally, the cross sections for transfer ionization are drawn in Fig. 8(c). The shapes of the IPGE and ACR cross sections are in noticeable agreement with the experimental one [32,33]. As for the previous cases, our approaches provide results in close agreement with the two-electron CTMC simulations of Wetmore and Olson [35]; all of them still overestimate the measurements. While various KW calculations seriously fail at all E, the energy-bounded approach of Cohen [20] strikingly succeeds in reproducing the experimental cross section despite the fact that both the KW and the energy-bounded methods rely on the use of similar constraining potentials which prevent one electron from getting too bounded while the other one is unphysically ionized.

IV. CONCLUSIONS

In this paper, we have proposed two active-electron CTMC models for ion-He collisions, inspired by classical molecular-dynamics studies [25–27] in which repulsion forces are smoothed using a Gaussian kernel approximation for the pointwise classical particles. Our first model uses N^2 independent pairs of Gaussian electrons (IPGE) and initial conditions are defined as a product of two identical microcanonical distributions corresponding to a He^+ state with effective energy E', so that the subsequent propagation of the Hamilton's equations, including the smoothed repulsion force, yields the correct first ionization potential of He. Our second model (ACR) rather draws from time-dependent mean-field theories and the repulsion force that one electron experiences stems from the average of binary forces with the N electrons belonging to the other set. Self-consistent microcanonical initial conditions have been built in this framework, but improved cross sections are obtained at low and intermediate impact energies if one mimics better the quantum electron densities, as is usual in one-electron collisional systems.

These models have been applied to p+He collisions. Noticeable stability of the computed cross sections with respect to the σ_r smoothing parameter has been obtained. For one-electron dynamical processes, both models yield quite accurate results in comparison to the available experimental data. Concerning two-electron transitions, our methods lead to well-shaped but overestimated cross sections. With respect to the mean-field ACR model, we mentioned that it can be due to an underestimation of the averaged e-e force when electrons localize around the nuclear centers as these approach or recede from each other, out from the molecular $Z=vt\sim 0$ region. A future stage of development of mean-field classical approaches should accordingly incorporate an averaging procedure which depends on the location of electrons on or between the nuclear centers. Within the IPGE framework, it does not seem feasible to correct for the underestimation of the e-e force as $r_{12}\rightarrow 0$ since it would imply the use of small σ_r smoothing parameters which do not allow stability of the unperturbed two-electron target.

However, we believe that the results shown in Figs. 7 and 8 indicate that our present two-electron models are competitive with previous classical methods, built from Hartree-Fock perspective [35], or including constraining potentials to impede unphysical autoionization [19,20,34]. The accuracy of these methods seems to increase with increasing projectile charge (despite the sensitivity of the Kirschbaum and Wilets procedure on the selected value of the constraining parameter); in this respect, our present models are promising and corresponding calculations, of considerable interest for fusion plasma research, will be performed. Further, the ACR model is particularly adapted to the study of multielectron dynamics since mean-field theory implies the propagation of (only) $m\times N$ Hamilton's equations, where m is the number of active electrons and N is the dimension of each electronic phase-space set. More complex targets than He can then be considered. Work along all these lines will be performed in the near future.

ACKNOWLEDGMENTS

This work has been partially supported by Project No. ENE2007-62934 from Dirección General de Investigación (Spain). F.G. acknowledges Fundacion Avelino López de Castro and Ciemat for their support and all authors thank H. Jouin for a careful reading of the paper.

[1] R. Abrines and I. C. Percival, Proc. Phys. Soc. London **88**, 861 (1966).
[2] R. E. Olson and A. Salop, Phys. Rev. A **16**, 531 (1977).
[3] D. J. W. Hardie and R. E. Olson, J. Phys. B **16**, 1983 (1983).
[4] R. L. Becker and A. D. MacKellar, J. Phys. B **17**, 3923 (1984).
[5] C. Illescas and A. Riera, Phys. Rev. A **60**, 4546 (1999).
[6] L. F. Errea, C. Harel, C. Illescas, H. Jouin, L. Méndez, B. Pons, and A. Riera, J. Phys. B **31**, 3199 (1998).
[7] J. Kuang and C. D. Lin, J. Phys. B **29**, 5443 (1996).
[8] T. Kirchner, H. J. Luedde, and M. Horbatsch, Recent Res. Dev. Phys. **5**, 433 (2004).
[9] L. F. Errea, F. Guzmán, C. Illescas, L. Méndez, B. Pons, A. Riera, and J. Suárez, Plasma Phys. Controlled Fusion **48**, 1585 (2006).
[10] R. J. Fonck, D. S. Darrow, and K. P. Jaehnig, Phys. Rev. A **29**, 3288 (1984).
[11] J. H. McGuire and L. Weaver, Phys. Rev. A **16**, 41 (1977).
[12] V. Sidorovich, J. Phys. B **14**, 4805 (1981).
[13] C. Illescas, B. Pons, and A. Riera, Phys. Rev. A **65**, 030703(R) (2002).
[14] M. B. Shah, C. McGrath, C. Illescas, B. Pons, A. Riera, H. Luna, D. S. F. Crothers, S. F. C. ORourke, and H. B. Gilbody, Phys. Rev. A **67**, 010704(R) (2003).
[15] C. O. Reinhold and C. A. Falcón, Phys. Rev. A **33**, 3859 (1986).
[16] R. K. Janev and M. McDowell, Phys. Lett. A **102**, 405 (1984).
[17] D. Elizaga *et al.*, J. Phys. B **32**, 857 (1999).
[18] L. F. Errea, J. D. Gorfinkiel, C. Harel, H. Jouin, A. Macías, L. Méndez, B. Pons, and A. Riera, J. Phys. B **33**, 3107 (2000).
[19] C. L. Kirschbaum and L. Wilets, Phys. Rev. A **21**, 834 (1980).
[20] J. S. Cohen, Phys. Rev. A **54**, 573 (1996).
[21] V. J. Montemayor and G. Schiwietz, Phys. Rev. A **40**, 6223 (1989).
[22] F. Guzmán, L. F. Errea, L. Méndez, B. Pons, and A. Riera, J. Phys.: Conf. Ser. **163**, 012069 (2009).
[23] B. H. Bransden and M. R. C. McDowell, *Charge Exchange and the Theory of Ion-Atom Collisions* (Clarendon Press, Oxford, 1992).
[24] H. Goldstein, *Classical Mechanics* (Addison-Wesley Academic Press, Orlando, 1954).
[25] E. J. Heller, J. Chem. Phys. **75**, 2923 (1981).
[26] T. Martinez, M. Ben-Nun, and R. Levine, J. Phys. Chem. **100**, 7884 (1996).
[27] M. Belkacem, F. Megi, P.-G. Reinhard, E. Suraud, and G. Zwicknagel, Phys. Rev. A **73**, 051201(R) (2006).
[28] B. H. Bransden and C. J. Joachain, *Physics of Atoms and Molecules* (Pearson Education, Harlow, England, 2003).
[29] L. F. Errea, C. Illescas, L. Méndez, B. Pons, A. Riera, and J. Suárez, Phys. Rev. A **70**, 052713 (2004).
[30] E. Clementi and C. Roetti, At. Data Nucl. Data Tables **14**, 177 (1974).
[31] N. Stolterfoht, R. D. DuBois, and R. D. Rivarola, *Electron Emission in Heavy Ion-Atom Collisions* (Springer, Berlin, 1977).
[32] M. B. Shah, P. McCallion, and H. B. Gilbody, J. Phys. B **22**, 3037 (1989).
[33] M. B. Shah and H. B. Gilbody, J. Phys. B **18**, 899 (1985).
[34] D. Zajfman and D. Maor, Phys. Rev. Lett. **56**, 320 (1986).
[35] A. E. Wetmore and R. E. Olson, Phys. Rev. A **38**, 5563 (1988).
[36] H. Slim, E. Heck, B. Bransden, and D. Flower, J. Phys. B **24**, 1683 (1991).
[37] H. Slim, E. Heck, B. Bransden, and D. Flower, J. Phys. B **24**, L421 (1991).
[38] T. G. Winter, Phys. Rev. A **44**, 4353 (1991).
[39] L. F. Errea, L. Méndez, and A. Riera, Z. Phys. D: At., Mol. Clusters **14**, 229 (1989).
[40] M. R. C. McDowell and J. P. Coleman, *Introduction to the Theory of Ion-Atom Collisions* (North-Holland, Amsterdam, 1970).
[41] J. Williams, Phys. Rev. **150**, 7 (1966).
[42] L. Toburen and Y. Nakai, Phys. Rev. **177**, 191 (1969).
[43] D. Belkić and I. Mančev, Phys. Scr. **47**, 18 (1993).
[44] C. D. Lin, Phys. Rev. A **19**, 1510 (1979).